# Mathematical and Numerical Properties of Control-Volume, Finite-Element Scheme for Reservoir Simulation

**Robert Eymard,** Laboratoire Central des Ponts & Chaussées, and
**Fernand Sonier,** SPE, Simulation & Modelling Consultancy Ltd.

## Summary

This paper presents the mathematical properties of a control-volume, finite-element (CVFE) scheme. We show that appropriate constraints on finite-element grids and convenient definitions for volumes and transmissibilities lead to a convergence property for the CVFE scheme. This convergence property proves that use of the CVFE scheme is mathematically correct for reservoir simulation. With the control-volume concept, the local balances of each component are fully satisfied. Because the discretized equations resulting from the scheme can be solved by classic methods, the CVFE scheme can be implemented easily in a general-purpose simulator. In the implementations in this paper, we use prismatic finite elements for 3D full-field simulations and triangles for 2D simulations. The grid is generated with automatic techniques, popular in structural engineering, resulting in numerical diffusion that is as isotropic as possible; therefore, grid-orientation effects are controlled and accuracy is easily improved through natural grid refinement. Examples show that, for the same accuracy, computational costs are lower for results obtained with the CVFE scheme than for those obtained with finite-difference grids. The CVFE scheme is an excellent alternative to flexible gridding techniques used in finite-difference simulators because the entire reservoir can be gridded as required, without use of special techniques for local grid modifications.

## Introduction

Because finite-element methods are naturally convenient for gridding areas with irregular boundaries and local refinements, several attempts have been made to use finite elements for reservoir simulation. Douglas[1] and Chavent *et al.*[2] used discontinuous and mixed finite elements for two-phase incompressible flows; Eymard *et al.*[3] used mixed hybrid finite elements, which lead to smaller linear systems, an advantage over previous methods; and Lemonier[4] reported the first attempt with the CVFE method.

In all these attempts, finite-element methods are used to solve a "pressure equation." Then, the conservation equations of all the components except one are sequentially solved by various techniques, all of which lead to control-volume methods. None of the methods used in these attempts has been generalized successfully to model realistic black-oil cases. This can be explained by the following: (1) no finite-element method exists for the Buckley-Leverett saturation equation, (2) use of different schemes for the pressure equation and the component conservation equation excludes correct balances for all the components, and (3) only schemes that keep all the balances correct have been shown to handle compressibility and thermodynamic phenomena.

On the other hand, the usual finite-difference methods[5-7] have been improved for more-complex physical processes (compositional, thermal, and chemical flood simulation) by use of fully implicit and implicit-pressure/explicit-saturation (IMPES) -coupled methods that provide perfect balances for all the components. Note that these usual finite-difference schemes are, in fact, control-volume, finite-difference (CVFD) schemes.



Original SPE manuscript received for review Feb. 28, 1993. Revised manuscript received April 14, 1994. Paper accepted for publication July 26, 1994. Paper (SPE 25267) first presented at the 1993 SPE Symposium on Reservoir Simulation held in New Orleans, Feb. 28–March 3.

Until recently, CVFE schemes have been shown to present the advantages of finite-element grids and fully coupled schemes. Examples of such applications to thermal and compositional simulation have been presented.[8-10] However, these papers have shown applications with no proof that the CVFE scheme is mathematically correct and convergent. The purpose of this paper is two-fold. First, we present the mathematical and numerical features of the CVFE scheme where some convergence properties are helpful for the definition of the fundamental concepts and the elimination of unsuitable considerations. Then, we present some applications to demonstrate the advantages of the CVFE scheme compared with classic CVFD methods. The Appendix summarizes the mathematical proof of the CVFE convergence property.

## CVFE Scheme

Refs. 5 through 7 give a complete description of reservoir equations in black-oil, thermal, and compositional cases, and Refs. 8 through 11 give detailed presentations of CVFE schemes. Because the CVFE scheme is presented in this paper from a conceptual point of view, the general conservation equation is expressed as

$$(\partial A/\partial t) - \nabla\left(\vec{kB}\nabla C\right) = 0. \quad \ldots\ldots\ldots\ldots\ldots\ldots\ldots\ldots (1)$$

In the most general case, the accumulation functions, $A$; the transport functions, $B$; and the potential functions, $C$, are nonlinear functions of pressure and of all the convective variables.

**Scheme Formulation.** Formulation of the scheme involves four steps.

1. The reservoir is gridded by elements, such as triangles and parallelograms (if a 2D model is available), or other polyhedral volumes (for 3D simulation). If the reservoir includes several rock types, each element must be homogeneous.

2. Test functions, $X_j(x)$, of any Point $x$ of the reservoir are defined for each Node $j$ of the grid (**Fig. 1**). These functions are, in the case of triangles in 2D or tetrahedrals in 3D, piecewise continuous linear functions ("chapeau" functions) for every Point $x$ of the reservoir that meet the essential property

$$\sum_j X_j(x) = 1. \quad \ldots\ldots\ldots\ldots\ldots\ldots\ldots\ldots\ldots\ldots (2)$$

Control volumes are located at the nodes of the grid with

$$v_j = \int_\Omega X_j(x)\mathrm{d}x. \quad \ldots\ldots\ldots\ldots\ldots\ldots\ldots\ldots\ldots\ldots (3)$$

Note that this definition can be made without any description of the boundaries of each control volume. However, such a description[9,10] does not yield any additional properties for the convergence of the scheme. Because of Eq. 2, the local and global volumes are naturally respected. In the case of triangles or tetrahedrals, each node of an element is respectively given one-third or one-quarter of the volume of this element.

Transmissibility values are defined by

$$T_{jk} = -\int_\Omega \nabla X_j(x)\cdot\vec{k}\nabla X_k(x)\mathrm{d}x. \quad \ldots\ldots\ldots\ldots\ldots\ldots\ldots (4)$$

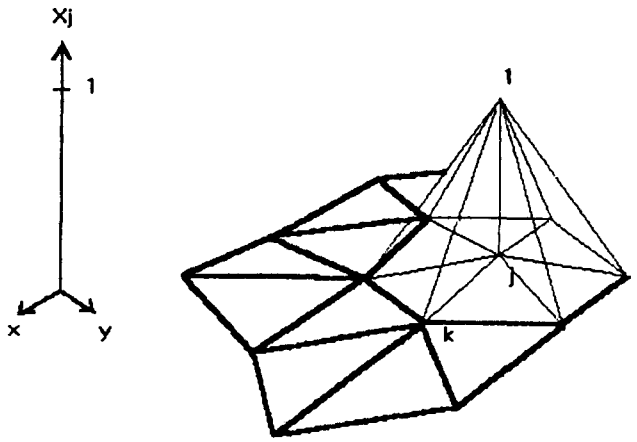


**Fig. 1—Test function $X_j$.**

The permeability tensor, $\vec{\vec{k}}$, can include nondiagonal terms, which is useful when tensors are generated by homogenization processes.

3. Eqs. 3 and 4 combined with Eq. 5, the equation for any component and any Node $j$ of the grid, define the CVFE scheme:

$$A_j^{n+1}v_j - A_j^n v_j - \Delta t^n \sum_{k \neq j} B_{jk}^m T_{jk}\left(C_k^{n+1} - C_j^{n+1}\right) = 0. \quad \ldots \quad (5)$$

In Eq. 5, the fully implicit scheme is obtained with $m = n + 1$ (the IMPES scheme can be obtained with $m = n$) and $B_{jk}^m = B_k^m$ if $T_{jk} \cdot (C_k^{n+1} - C_j^{n+1})$ is positive; otherwise, $B_{jk}^m = B_j^m$. Flows between two control volumes do not involve the unknowns of any other control volume, even for the potential gradient evaluation.

4. The nonlinear Eq. 5 is solved for any $j$ and $n$. Classic Newton-Raphson methods are used, and the change of thermodynamic state is computed at each iteration.[5-7,12]

**Scheme Properties.** The mathematical background that is relevant for the study of the CVFE scheme includes weak formulas and the weak star topology for bounded functions (see the Appendix). As a result, the CVFE scheme is such that, for a sequence of grids whose space-step size decreases to zero, the approximate solutions converge to the exact solution. Some understanding can be drawn from CVFE convergence properties.

1. As a consequence of applying the CVFE scheme to the conservation of all the components, a classic finite-element method is used to compute pressures for the linear case.

2. Convergence of the CVFE scheme does not imply in any way Taylor developments for potential terms (to obtain a local consistency with the Laplace operator everywhere). In addition, use of more than two potential values in the flow term expression between two control volumes can lead to instabilities in the convective variables.

3. The definition of the CVFE scheme by Eqs. 3 through 5 does not need any justification (geometry, integration, and volume interfaces) other than proof of the scheme convergence. The scheme defines discrete values for unknowns, and approximate solutions can be taken as linear combinations of continuous test functions; infinite sets of functions (discontinuous or not) can lead to the same discrete values by integration with the relevant test functions.

4. The proof of convergence requires that all element angles be less than $\pi/2$ (Hypothesis 2 in the Appendix) so that all the transmissibilities are non-negative. Numerically, however, some instability in saturation occurs in elements where the inequality $T_{jk} \geq 0$ is not honored.

**Triangulation Algorithm and Grid-Orientation Effects.** The main cause of grid-orientation effects is that an anisotropic error resulting from the first-order space approximation of flow increases along the specific direction of a grid (this is a result of convective phenomena, not of the pressure scheme). For example, in the case of a grid made with squares cut into two triangles, the resulting transmissibility values are the CVFD values (the diagonal transmissibilities are equal to zero because the gradient of the test functions are orthogonal). So in this case, use of the CVFE scheme does not prevent grid-orientation effects.

To avoid anisotropies resulting from specific directions in the grid, an algorithm of automatic triangulation[13] has been implemented in our code together with a smoothing calculation. In this algorithm, a sequence of nodes, initialized at the boundary, is progressively reduced and modified during element generation until it includes only three nodes. This algorithm can be summarized by the following steps.

1. The reservoir boundary is discretized.

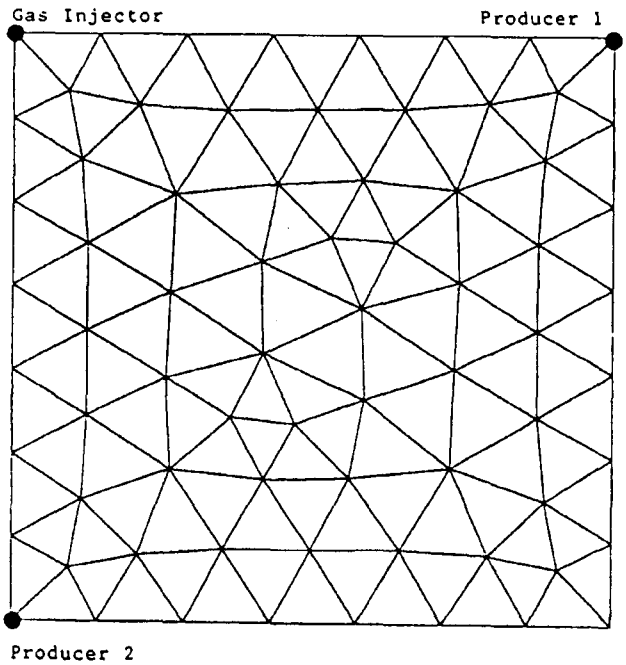


**Fig. 2—CVFE grid with 72 nodes per layer, Eighth SPE Comparative Solution Project.[15]**

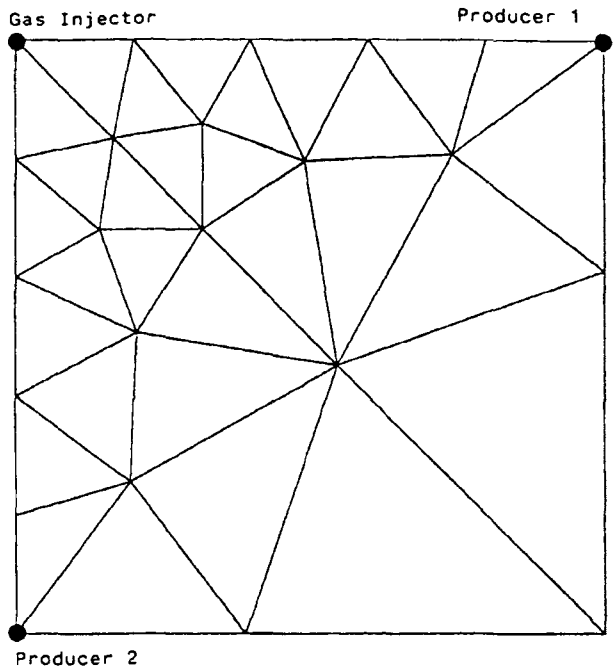


**Fig. 3—CVFE grid with 23 nodes per layer, Eighth SPE Comparative Solution Project.[15]**

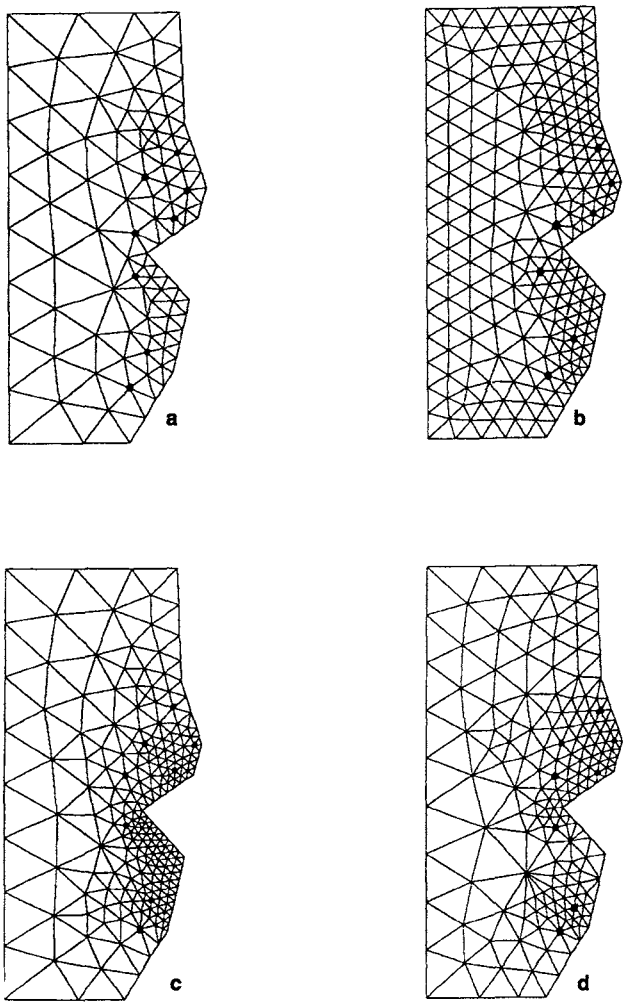


**Fig. 4—Examples of automatic grid generation for CVFE scheme: (a) coarse grid, (b) fine grid, (c) coarse grid with one refinement, and (d) coarse grid with two refinements.**

2. A sequence of nodes is initialized by this discretized boundary.

3. For any sub-sequence of three nodes, if the resulting angle is acute, an element is generated with these nodes, and the second of these three nodes is removed from the sequence.

4. For any sub-sequence of three nodes, if the resulting angle is obtuse, a new point is generated inside the not-yet-gridded area; this point replaces the second of the three nodes in the sequence, and two elements are generated.

5. Steps 3 and 4 are repeated until the sequence includes only three nodes.

6. Triangular refinement[4] is applied to the grid (triangles are divided by 4 or 2). This process preserves the consistency of the connections, and no special techniques have to be applied to reduce discretization errors.

7. The grid is then smoothed, and edges are moved if larger angles can be obtained.

This algorithm leads to regular grids with no specific orientation, and Delauney triangulations then can be obtained easily. The examples show the facilities for local refinement.

**Boundary Conditions.** The boundary has to be discretized by edges of triangles. Therefore, in case of boundary nodes, the control volumes are located only at one side of the boundary (**Figs. 2 through 4**). Any type of boundary condition can be handled.

Pressure value is imposed in a boundary control volume. Because this Dirichlet's condition must be physically compatible with the variations of the other unknowns of the control volume, it can be satisfied if the conservation equations of all the components are solved by Newton's method. Then, the resulting increments of pressure at this boundary have to be set to zero.

Flow conditions are imposed. This Von Neumann's condition is satisfied by increasing the right sides of the conservation equations with the imposed values. Therefore, zero-flow conditions can be obtained naturally by solving the CVFE conservation equations of a boundary control volume.

**Well Index.** In the CVFE scheme, as in finite-difference schemes, wells are implemented in control volumes. The monophasic linear 2D, incompressible equation for Node $j$, in which a well is implemented, is

$$\sum_{k \neq j} T_{jk}(p_k - p_j) = q. \quad \ldots\ldots\ldots\ldots\ldots\ldots\ldots\ldots\ldots\ldots (6)$$

Following Peaceman's[14] method, the expression of well index can be obtained when boundary conditions are such that the calculated pressures agree with

$$p(r) = p_w + (q/2\pi k_H)\ln(r/r_w). \quad \ldots\ldots\ldots\ldots\ldots\ldots\ldots\ldots (7)$$

With Eqs. 6 and 7, the pressure in Node $j$ must agree with

$$\sum_{k \neq j} T_{jk}\left[p_w + \frac{q}{2\pi k_H}\ln\left(\frac{r_k}{r_w}\right) - p_j\right] = q. \quad \ldots\ldots\ldots\ldots\ldots\ldots (8)$$

The well index, $I_w$, is defined by $I_w = q/(p_j - p_w)$. This yields

$$I_w = 2\pi k_H \Big/ \left[\ln(r_b/r_w) - \left(2\pi k_H \Big/ \sum_{k \neq j} T_{jk}\right)\right], \quad \ldots\ldots\ldots (9)$$

$$\text{where } r_b = \exp\left[\sum_{k \neq j} T_{jk}\ln(r_k) \Big/ \sum_{k \neq j} T_{jk}\right]. \quad \ldots\ldots\ldots\ldots (10)$$

Eq. 9 for $I_w$ is the same as Peaceman's formula for the finite-difference case.

## Numerical Results

**Eighth Comparative Solution Project Problem.**[15] This problem is a 3D simulation of oil production and gas injection in a four-layer reservoir. Ref. 15 gives the complete data. Because the problem was a comparison of regular finite-difference methods and flexible gridding techniques, elimination of any grid-orientation effects in the regular discretization simulation was necessary. For this purpose, regular fine-grid simulations have been performed with a five-point as well as with a nine-point scheme.

Because the purpose of the project problem was to reduce the number of gridblocks as much as possible within an accuracy criterion (results should match the results from a fine simulation within 10%), several CVFE triangular grids were generated and used: from 17 to 72 nodes per layer. **Table 1** provides details on results for four selected schemes.

***Scheme 1: REG-FD-5P.*** This is a $10 \times 10 \times 4$-node, regular finite-difference, five-point scheme.

***Scheme 2: REG-FD-9P.*** A $10 \times 10 \times 4$-node, regular finite-difference, nine-point scheme, which is used as the reference scheme.

***Scheme 3: CVFE-72.*** This is a $72 \times 4$-node, regular CVFE-scheme grid (Fig. 2).

***Scheme 4: CVFE-23.*** This is a $23 \times 4$-node, CVFE-scheme grid (Fig. 3).

**Fig. 5** shows breakthrough times and initial GOR at Producer 1 for these schemes. From Table 1 and Fig. 5, we can determine the following.

With the usual finite-difference five-point scheme, gas breakthrough time is influenced by grid-orientation effects; the 2,000-scf/STB GOR is reached at 800 days for Scheme 1 and at only 940 days for Scheme 2. Results from Scheme 1 do not meet the required accuracy criterion.

| TABLE 1—DATA FOR EIGHTH SPE COMPARATIVE SOLUTION PROJECT[15] | | | | |
|---|---|---|---|---|
| | Scheme 1 REG-FD-5P | Scheme 2 REG-FD-9P | Scheme 3 CVFE-23 | Scheme 4 CVFE-72 |
| | Time (days) | | | |
| Producer 1 | | | | |
| At GOR of 1,500 scf/STB | 740 | 880 | 810 | 890 |
| At GOR of 2,000 scf/STB | 800 | 940 | 915 | 950 |
| At GOR of 10,000 scf/STB | 2,170 | 2,190 | 2,170 | 2,215 |
| Producer 2 | | | | |
| At GOR of 1,500 scf/STB | 700 | 840 | 770 | 845 |
| At GOR of 2,000 scf/STB | 750 | 890 | 865 | 900 |
| At GOR of 10,000 scf/STB | 2,100 | 2,120 | 2,100 | 2,130 |
| Injector | Pressure (psia) | | | |
| At 1,000 days | 4,954 | 5,050 | 5,006 | 5,066 |
| At 2,400 days | 3,440 | 3,499 | 3,448 | 3,550 |
| | Run-Time Ratio | | | |
| | 1.0 | 1.32 | 0.25 | 0.97 |

Grid-orientation effects do not occur in the CVFE schemes: the 2,000-scf/STB GOR is reached at 950 and 915 days for Schemes 3 and 4, respectively, compared with 940 days for Scheme 2.

Results of Schemes 2 through 4 are very similar (differences are < 3% throughout the simulations). Taking the central-processing-unit (CPU) time of Scheme 1 as a reference, the CPU-time ratios are 1.32, 0.97, and 0.25 for Schemes 2, 3, and 4, respectively. For this particular problem, Scheme 4 with only 23 nodes per layer demonstrates the natural local grid-refinement capability of the CVFE scheme. Within the accuracy criteria, grid numbers and computer-time are reduced by 4 and 5.4, respectively. Results of Schemes 2 and 3, which can be considered as the two fine, regular grids for this problem, are very close, indicating that the CVFE scheme can be used not only for special simulations, such as local grid refinement, but also for any type of simulation work. Note that similar results have been found by extending this problem to three-mobile-phase, black-oil problems as well as to five-component equation-of-state (EOS) compositional problems.

**Example of Full-Field CVFE Grids.** Although numerous papers on special techniques for grid refinement were published, Ref. 16 gives the only full-field example comparing regular and composite gridding. Obviously, since presentation of that paper, similar composite gridding techniques have been improved. The only purpose of this section is to show another technique for gridding a full-field reservoir. Ref. 16 gives a description of the example field study and discusses the results.

Briefly, the reservoir is limited by impermeable faults in the north and south and by a large aquifer in the west. Fig. 7 of Ref. 16 shows the isobath map at reservoir top and the location of the eight wells. Fig. 8 of Ref. 16 shows three ways of gridding the reservoir: (1) a coarse grid with 336 blocks/layer, (2) a partial refinement of the coarse grid for a better representation of the reservoir with 819 blocks/layer, and (3) a local refinement of the coarse grid with the ZOOM model with 509 active blocks. Results (from Figs. 10 and 11 of Ref. 16) on water cut show that the coarse grid is not accurate enough to match actual results and that the ZOOM technique gives good results with much fewer blocks than the fine grid.

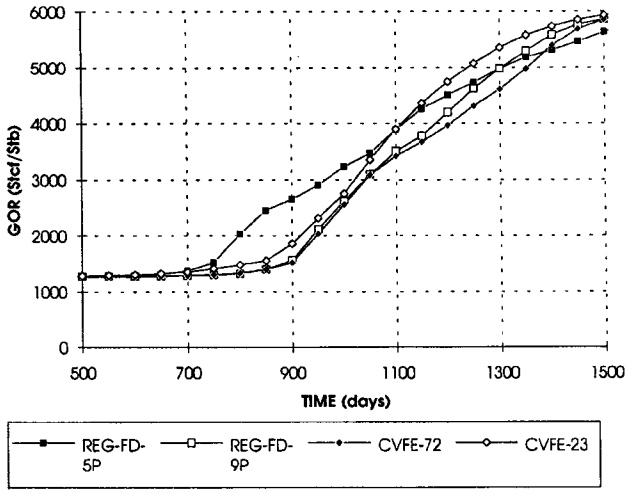


**Fig. 5—GOR vs. time for Producer 1, Eighth SPE Comparative Solution Project.[15]**

Comparison of water-cut results with the CVFE scheme and different numbers of nodes would be a good idea. However, while the geometry and locations of the wells are quite accurate, the other data are not good enough (e.g., inconsistent data for PV's and production). Therefore, reproduction of Ref. 16 results was not possible.

To illustrate the flexibility of the automatic grid generation, we show some examples in Fig. 4 that follow the same approach as in Ref. 16. Fig. 4a is a coarse grid with 104 nodes per layer; the greatest grid-size ratio is 3.5. Fig. 4b is a fine grid with 251 nodes per layer, and the greatest grid-size ratio is 2. Fig. 4c shows the coarse grid of the Fig. 4a with one local grid refinement in the oil zone. This grid has 222 nodes per layer, and the greatest grid-size ratio is 7. Fig. 4d shows the coarse grid with two local grid refinements: one around the two wells in the south part of the field and one around the other wells. The nodes per layer is reduced to 180. Fig. 4 shows that only the active area has to be gridded and that grid refinement can be performed at any location while regular connections are kept. The only caution is that the grids must be checked to ensure that all the transmissibility coefficients are positive.

Note that several black-oil and EOS compositional problems have been simulated with these four gridding examples. Differences in results are not significant enough to be shown because all the wells are located on the top of the reservoir, which makes this example behave more like a water/oil problem with a large aquifer.

## Conclusions

1. Stability of the CVFE scheme (which can be used for any compressible, miscible, compositional, or thermal 3D reservoir simulation problem) is a result of honoring of local balances for all the components.
2. The convergence of the CVFE scheme has been proved, under some hypotheses.
3. The CVFE scheme allows the use of automatic grid generation for creation of optimal gridding schemes that eliminate simulation errors caused by grid-orientation effects and an incorrect grid around reservoir heterogeneities and wells.
4. All current simulation work can be done with a CVFE simulator because the CVFE scheme has several mathematical and numerical advantages over the CVFD scheme and no disadvantages. The only requirement for a CVFE simulator is the availability of finite-element pre- and postprocessors.

## Nomenclature

$A$ = accumulation function
$B$ = convection function

$B_V$ = discrete variation of saturation
$C$ = potential function
$D$ = constant in stability condition
$E$ = function of triangulation and timestep size
$F$ = test function
$g$ = volumetric flow at boundary
$h$ = space-step size
$H$ = constant
$I_w$ = well index
$\vec{\vec{k}}$ = permeability tensor
$k_H$ = horizontal permeability, $L^2$
$K$ = bound of quadratic variation of saturation
$\vec{n}$ = unit vector, normal at boundary
$N$ = integer value such that $N \cdot \Delta t$ is large enough
$p$ = pressure, $m/Lt^2$
$p_w$ = wellbore bottomhole pressure, $m/Lt^2$
$q$ = well rate, $L^3/t$
$r$ = distance to well, L
$r_b$ = drainage radius, L
$r_w$ = well radius, L
$S$ = saturation
$\overline{S}$ = average saturation
$S_o$ = initial saturation
$\Delta t$ = timestep size, t
$T$ = transmissibility
$t$ = time variable, t
$V_h$ = space of piecewise linear functions
$x,y$ = space coordinates
$X$ = regular test function for pressure
$X_j$ = chapeau-test function at Node $j$
$\gamma$ = boundary coordinate
$\Gamma$ = reservoir boundary
$v$ = control volume, $L^3$
$\rho$ = given real value between 0 and 1
$\phi$ = regular test function
$\Omega$ = reservoir

**Subscripts**

$h$ = step size
$i,j,k$ = gridblock indices
$m,n$ = timestep indices

**Superscripts**

$m,n$ = timestep indices


## Acknowledgment

We thank T. Gallouët for useful discussions during the course of this research.


## References


1. Douglas, J. Jr: "Numerical Methods for the Flow of Miscible Fluids in Porous Media," *Numerical Methods in Coupled Systems*, R.W. Lewis, P. Betess, and E. Hinton (eds.), John Wiley & Sons Inc., New York City (1984) 405–39.
2. Chavent, G. *et al.*: "Discontinuous and Mixed Finite Elements for Two-Phase Incompressible Flow," *SPERE* (Nov. 1990) 567; *Trans.*, AIME, **289.**
3. Eymard, R., Gallouët, T., and Joly, P.: "Hybrid Finite Element Techniques for Oil Recovery Simulation," *Computer Methods in Applied Mechanics &. Eng.* (1989) **74,** 83.
4. Lemonnier, P.A.: "Improvement of Reservoir Simulation by a Triangular Discontinuous Finite-Element Method," paper SPE 8249 presented at the 1979 SPE Annual Technical Conference and Exhibition, Las Vegas, Sept. 23–26.
5. Young, L.C. and Stephenson, R.E.: "A Generalized Compositional Approach for Reservoir Simulation," *SPEJ* (Oct. 1983) 727.
6. Coats, K.H.: "In-Situ Combustion Model," *SPEJ* (Dec. 1980) 533.
7. Sonier, F. and Eymard, R.: "A New Simulator for Naturally Fractured Reservoirs," paper SPE 16006 presented at the 1987 SPE Reservoir Simulation Symposium, San Antonio, Feb. 1–4.
8. Rozon, J.: "A Generalized Finite-Volume Discretization Method for Reservoir Simulation," paper SPE 18414 presented at the 1989 SPE Reservoir Simulation Symposium, Houston, Feb. 6–8.
9. Forsyth, P.A.: "A Control-Volume Finite-Element Method for Local Mesh Refinement in Thermal Reservoir Simulation," *SPERE* (Nov. 1990) 561; *Trans.*, AIME, **289.**
10. Fung, L. S.-K., Hiebert, A.D., and Nghiem, L.: "Reservoir Simulation With a Control-Volume Finite-Element Method," *SPERE* (Aug. 1992) 349.
11. Faille, I.: "A Control Volume Method to Solve an Elliptic Equation on a Two-Dimensional Irregular Mesh," *Computer Methods in Applied Mechanics & Eng.* (1992) **100,** 275.
12. Joly, P. and Eymard, R.: "Preconditioned Biconjugate Gradient Methods for Numerical Reservoir Simulation," *J. Comp. Physics* (1990) **91,** No. 2.
13. Garcia, M.: "Application à l'exploitation du sous-sol des interfaces: systèmes de CAO—mailleurs 3D—codes numériques," PhD dissertation of Ecole Natl. Supérieure des Mines de Paris, Paris (1988).
14. Peaceman, D.W.: "Interpretation of Wellblock Pressures in Numerical Reservoir Simulation," *SPEJ* (June 1978) 183; *Trans.*, AIME, **265.**
15. Quandalle, P.: "Eighth SPE Comparative Solution Project: Gridding Techniques in Reservoir Simulation," paper SPE 25263 presented at the 1993 SPE Symposium on Reservoir Simulation, New Orleans, Feb. 28–March 3.
16. Quandalle, P. and Besset, P.: "The Use of Flexible Gridding for Improved Reservoir Modeling," paper SPE 12239 presented at the 1983 SPE Reservoir Simulation Symposium, San Francisco, Nov. 16–18.
17. Gallouët, T., Herbin, R., and Champier, S.: "Convergence of an Upstream Finite Volume Scheme on a Triangular Mesh for a Nonlinear Hyperbolic Equation," *Numeris Math.* (1993) **66,** 139.
18. Gallouët, T. and Herbin, R.: "A Uniqueness Result for Measure-Valued Solution of a Nonlinear Hyperbolic Equation" *J. Diff. Int. Equations* (1994).
19. Eymard, R.: *Mémoire d'habilitation à diriger des recherches*, U. de Savoie, Chambéry (1992).
20. Eymard, R. and Gallouët, T.: "Convergence d'un schema de type elements finis volumes finis pour un systéme formé d'une equation elliptique et d'une equation hyperbolique," *Mathematical Modelling & Numerical Analysis* (1993) **27,** No. 7, 843.


## Appendix—Synopsis of Proof of Convergence

Here, we show the convergence of the CVFE scheme in the case of two-phase, 2D or 3D incompressible flow, without gravity and capillarity effects, assuming the total mobility as a constant and the fractional flow as a linear function. The theoretical frame of a nonconstant total mobility case seems to be much more difficult. The purpose of this Appendix is to give the exact importance of each concept in the convergence of the CVFE scheme.

The point of this proof is inequality (Eq. A-30), which is a kind of weak, total variation, decreasing estimation.[17] This kind of estimation is also essential in the nonlinear case.[18] Handling source terms adds no difficulty; for simplicity of presentation, they are not included. Refs. 19 and 20 give all the detailed calculations.

**Convergence Properties.** The physical problem, presented in the introduction of this Appendix, leads to the following system of equations for any Point $x$ of the reservoir, $\Omega$, and at any time $t \geqq 0$.

$$(\partial S/\partial t)(x,t) - \nabla[S(x,t)\nabla p(x)] = 0 \quad \ldots\ldots\ldots\ldots\ldots \text{(A-1)}$$

and $$\Delta p(x) = 0. \quad \ldots\ldots\ldots\ldots\ldots\ldots\ldots\ldots\ldots\ldots \text{(A-2)}$$

Flow boundary conditions hold at any Point $\gamma$ of the boundary, $\Gamma$:

$$\nabla p(\gamma)\cdot\vec{n} = g(\gamma). \quad \ldots\ldots\ldots\ldots\ldots\ldots\ldots\ldots \text{(A-3)}$$

Because of the hypothesis of incompressibility of fluids, Eq. A-3 is true only if $\int_\Gamma g(\gamma)d\gamma = 0$.

Let $\Gamma^+$ represent the set of Points $\gamma$ of $\Gamma$ so that $g(\gamma) \geqq 0$. For any $\gamma$ of $\Gamma^+$, another boundary condition is given for the saturations:

$$S(\gamma,t) = \overline{S}(\gamma,t). \quad \ldots\ldots\ldots\ldots\ldots\ldots\ldots\ldots \text{(A-4)}$$

Finally, an initial condition is given for the saturation, $S(x, 0)$, for any Point $x$ of $\Omega$:

$$S(x,0) = S_o(x). \quad \text{(A-5)}$$

Values taken by functions $\bar{S}(\gamma,t)$ and $S_o(x)$ belong to Interval [0,1].

Because no regularity assumption can be made on saturation functions, Eq. A-1 can be considered only in the following weak meaning: the function $S(x,t)$ must be valued in Interval [0,1] and agree with

$$\int_0^\infty \int_\Omega S(x,t)\left[\frac{\partial\phi}{\partial t}(x,t) - \nabla p(x)\cdot\nabla\phi(x,t)\right]\mathrm{d}x\mathrm{d}t + \int_\Omega S_o(x)\phi(x,0)\mathrm{d}x + \int_0^\infty \int_{\Gamma^+} \bar{S}(\gamma,t)\phi(\gamma,t)g(\gamma)\mathrm{d}\gamma = 0 \quad \text{(A-6)}$$

for any regular function $\phi(x,t)$ with a bounded time support and so that for any Point $\gamma$ of the boundary, $\phi(\gamma,t)=0$ if $\gamma$ is not in $\Gamma^+$. One can notice that in Eq. A-6, derivatives are only applied to the regular function $\phi$.

Eq. A-2 is true in the same way as the classic variational formula for any regular test function $X(x)$,

$$\int_\Omega \nabla p(x)\cdot\nabla X(x)\mathrm{d}x - \int_\Gamma X(\gamma)g(\gamma)\mathrm{d}\gamma = 0. \quad \text{(A-7)}$$

If no additional hypotheses are made on the function $g$, the regularity properties of the solution to Eq. A-7 are not sufficient to deduce the existence of the solution to Eq. A-6 with the method of characteristics. We provide this existence property in this paper.

The behaviors of approximations $S_h$ and $p_h$ of $S$ and $p$ have to be carefully specified when space-step size, $h$, decreases. The first properties of convergence that are expected from the scheme follow.

***Weak Star Convergence for Saturation.*** For any function $F(x,t)$ so that $\int_0^\infty \int_\Omega |F(x,t)|\mathrm{d}x\mathrm{d}t < \infty$,

$$\lim_{h\to 0} \int_0^\infty \int_\Omega [S(x,t) - S_h(x,t)]F(x,t)\mathrm{d}x\mathrm{d}t = 0. \quad \text{(A-8)}$$

A stronger property of convergence can be obtained with entropy definitions[17]; however, because it yields more mathematical background such a result is not presented here.

***Strong Convergence for Pressure.***

$$\lim_{h\to 0} \int_\Omega \left\{[p(x) - p_h(x)]^2 + [\nabla p(x) - \nabla p_h(x)]^2\right\}\mathrm{d}x = 0. \quad \text{(A-9)}$$

**Space Discretization.** For any $h>0$, triangular grid elements can be defined that verify two hypotheses: (1) the smallest and greatest sizes within the set of elements are respectively bounded by two linear functions of $h$, and the smallest angle of the elements is greater than the same constant for any $h$; and (2) the greatest angle within the set of elements is smaller than $\pi/2$.

The chapeau-test function at Node $j$ is represented by $X_j(x)$. The following property is available for any Point $x$:

$$\sum_j X_j(x) = 1. \quad \text{(A-10)}$$

For each Node $j$, a control volume is defined by

$$v_j = \int_\Omega X_j(x)\mathrm{d}x. \quad \text{(A-11)}$$

Because of Eqs. A-10 and A-11, the reservoir porous volume is preserved. The transmissibility, $T_{jk}$, between $v_j$ and $v_k$ is defined by

$$T_{jk} = -\int_\Omega \nabla X_j(x)\cdot\nabla X_k(x)\mathrm{d}x. \quad \text{(A-12)}$$

Because of Hypothesis 2, $T_{jk}>0$.

For any Node $j$, a source term is defined by $g_j = \int_\Gamma X_j(\gamma)g(\gamma)\mathrm{d}\gamma$; if $j$ is not located at the boundary of $\Omega$, then $g_j=0$.

**Pressure Finite-Element Scheme.** With the space discretization, the finite-element approximation, $p_h$, of $p$ is defined by

$$p_h(x) = \sum_j p_j X_j(x). \quad \text{(A-13)}$$

This function is chosen so that it satisfies the variational formulation (Eq. A-7) for all test functions $X_j$. Then, the coefficients $p_j$ are the solution of the linear system

$$\sum_k T_{jk}(p_k - p_j) + g_j = 0. \quad \text{(A-14)}$$

The existence and uniqueness of a function $p$ solution of Eq. A-7 is a classic result. Because of Hypothesis 1, Eq. A-9 is a well-known result of the finite-element theory. Therefore, a fundamental property of CVFE scheme is that it leads to a strong property of convergence for pressure.

**Time Discretization.** Let $g_j^+$ be defined by

$$g_j^+ = \int_\Gamma X_j(\gamma)\max[g(\gamma),0]\mathrm{d}\gamma \quad \text{(A-15)}$$

and $g_j^- = g_j^+ - g_j$. Let $\rho$ be a given real value so that $0<\rho<1$. For any $h>0$, a value $\Delta t$ is chosen so that for several Nodes $j$,

$$\Delta t \leqq (1-\rho)\frac{v_j}{\sum_{k,p_k<p_j} T_{jk}(p_j - p_k) + g_j^-}. \quad \text{(A-16)}$$

Eq. A-16 is a stability condition; if some regularity conditions are given on the Boundary $\Gamma$ and on the function $g$, Eq. A-16 leads to the existence of a constant $D$ so that $\Delta t < Dh$.

**Saturation Control-Volume Scheme.** For any Node $j$, let $S_j^o$ and $\bar{S}_j^n$ be defined by

$$S_j^o = \frac{1}{v_j}\int_\Omega X_j(x)S_o(x)\mathrm{d}x. \quad \text{(A-17)}$$

$$\bar{S}_j^n \cdot \int_\Gamma X_j(\gamma)\mathrm{d}\gamma = \frac{1}{\Delta t}\int_{n\Delta t}^{n\Delta t+\Delta t}\int_\Gamma X_j(\gamma)\bar{S}(\gamma,t)\mathrm{d}\gamma\mathrm{d}t. \quad \text{(A-18)}$$

The CVFE scheme for saturation equation is given by

$$v_j(S_j^{n+1} - S_j^n) - \Delta t\left[\sum_k T_{jk}S_{jk}^n(p_k - p_j) + \bar{S}_j^n g_j^+ - S_j^n g_j^-\right] = 0 \quad \text{(A-19)}$$

where, if $p_k > p_j$,

$$S_{jk}^n = S_k^n; \quad \text{(A-20a)}$$

otherwise, $S_{jk}^n = S_j^n$. (A-20b)

$S_h(x,t)$ is then defined by $\sum_j S_j^n X_j(x)$ for any time $t$ so that $n\Delta t \leqq t < (n+1)\Delta t$.

**Stability Property on Saturation Approximations.** Because of Eqs. A-16, A-19, and A-20, we can see that for any Node $j$ and any $n \geqq 0$,

$$0 \leqq S_j^n \leqq 1. \quad \ldots\ldots\ldots\ldots\ldots\ldots\ldots\ldots \text{(A-21)}$$

Eq. A-21 is essential from a physical point of view and also because it leads to the existence of a function, $S(x,t)$, that verifies Eq. A-8 for a sub-sequence of $S_h(x,t)$; the function $S$ is assumed to be a weak star limit of a sub-sequence of $S_h$. With the proof that this function $S$ satisfies Eq. A-6, the scheme will converge.

**Proof Steps.** Let $\phi$ be a given regular function with a bounded time support so that for any Point $\gamma$ of the boundary, $\phi(\gamma,t)=0$ if $\gamma$ is not in $\Gamma^+$. Eq. A-6 can be obtained when proof of the two following steps is provided.

***Step 1.*** Let $E_{oh}$ be defined by

$$E_{oh} = \sum_{n=0}^{\infty} \sum_j \int_\Omega v_j \left(S_j^{n+1} - S_j^n\right) \frac{X_j(x)}{v_j} \phi(x,t^n) \mathrm{d}x. \quad \ldots\ldots \text{(A-22)}$$

Then,

$$\lim_{h \to 0} E_{oh} = -\int_0^\infty \int_\Omega S(x,t) \frac{\partial \phi}{\partial t}(x,t) \mathrm{d}x \mathrm{d}t - \int_\Omega S_o(x) \phi(x,0) \mathrm{d}x.$$

$$\ldots\ldots\ldots\ldots\ldots\ldots \text{(A-23)}$$

***Step 2.*** Let $E_{1h}$ be defined by

$$E_{1h} = \sum_{n=0}^{\infty} \sum_j \int_\Omega \Delta t \left[\Sigma_k T_{jk} S_{jk}^n \left(p_k - p_j\right) + g_j^+ S_j^n - g_j^- S_j^n\right]$$

$$\times \left[X_j(x)/v_j\right] \phi(x,t^n) \mathrm{d}x. \quad \ldots\ldots\ldots\ldots\ldots\ldots \text{(A-24)}$$

Then,

$$\lim_{h \to 0} E_{1h} = -\int_0^\infty \int_\Omega S(x,t) \nabla p(x) \cdot \nabla \phi(x,t) \mathrm{d}x \mathrm{d}t$$

$$+ \int_0^\infty \int_\Gamma \bar{S}(\gamma,t) \phi(\gamma,t) g(\gamma) \mathrm{d}\gamma \mathrm{d}t. \quad \ldots\ldots\ldots\ldots\ldots \text{(A-25)}$$

Because $E_{oh} - E_{1h} = 0$, with Eq. A-19 of the saturation scheme, Eq. A-6 results from Eqs. A-23 and A-25. Proof of Eq. A-23 is easy to get; however, proof of Eq. A-25 is more difficult. It can be split into three substeps.

*Substep 1.* Let $E_{2h}$ be defined by

$$E_{2h} = \sum_{n=0}^{\infty} \Delta t \left[\sum_{j,k,p_j > p_k} \left(S_j^n - S_k^n\right)\left(p_j - p_k\right) \int_\Omega \nabla X_j(x) \cdot \nabla X_k(x) \right.$$

$$\left. \times \phi(x,t^n) \mathrm{d}x + \sum_j \left(S_j^n - \bar{S}_j^n\right) \int_\Gamma X_j(\gamma) \phi(\gamma,t^n) g(\gamma) \mathrm{d}\gamma \right].$$

$$\ldots\ldots\ldots\ldots\ldots\ldots \text{(A-26)}$$

Then,

$$\lim_{h \to 0} E_{2h} = \int_0^\infty \int_\Omega S(x,t) \nabla p(x) \cdot \nabla \phi(x,t) \mathrm{d}x \mathrm{d}t$$

$$- \int_0^\infty \int_\Gamma \bar{S}(\gamma,t) \phi(\gamma,t) g(\gamma) \mathrm{d}\gamma \mathrm{d}t. \quad \ldots\ldots\ldots\ldots\ldots \text{(A-27)}$$

*Substep 2.* Let $N$ be the smallest integer value so that for any $t \geqq N \cdot \Delta t$ and any $x$, $\phi(x,t)=0$. Let $N = T/\Delta t$. Let $B_{V_h}$ be defined by

$$B_{V_h} = \Delta t \sum_{n=0}^{N} \sum_{j,k,p_j > p_k} T_{jk}\left(p_j - p_k\right) \left|S_j^n - S_k^n\right|$$

$$+ \Delta t \sum_{n=0}^{N} \sum_j g_j^+ \left|S_j^n - \bar{S}_j^n\right|. \quad \ldots\ldots\ldots\ldots\ldots\ldots \text{(A-28)}$$

Then, a constant $C$ is included so that for any $h$,

$$\left|E_{1h} + E_{2h}\right| \leqq Ch B_{V_h}. \quad \ldots\ldots\ldots\ldots\ldots\ldots\ldots \text{(A-29)}$$

*Substep 3.* A constant $H$, independent of $h$, is included so that for any $h$,

$$B_{V_h} \leq H h^{-1/2}. \quad \ldots\ldots\ldots\ldots\ldots\ldots\ldots\ldots \text{(A-30)}$$

Eq. A-25 results easily from the combination of Eqs. A-27, A-29, and A-30. Proof of Eq. A-27 can be made by use of the regularity of $\phi$ and Eqs. A-7 and A-14; the convergence property for pressures (Eq. A-9) is explicitly used. Proof of Eq. A-29 is easy to show with the Hypothesis 2 for grids and the regularity of $\phi$.

Finally, we can prove Eq. A-30 by the following method. First, we multiply Eq. A-19 by $S_j^n$. Then, we sum Indices $j$ and $n$. Finally, we use the upstream weighting scheme (Eq. A-20), Hypothesis 1, the variational equation (Eq. A-14), and the stability condition (Eq. A-16) to show the existence of a constant, $K$, so that

$$\Delta t \sum_{n=0}^{N} \sum_{j,k,p_j > p_k} T_{jk}\left(p_j - p_k\right)\left(S_j^n - S_k^n\right)^2$$

$$+ \Delta t \sum_{n=0}^{N} \sum_j g_j^+ \left(S_j^n - \bar{S}_j^n\right)^2 \leqq K. \quad \ldots\ldots\ldots\ldots\ldots \text{(A-31)}$$

Then, Eq. A-30 is obtained from Eq. A-31 by the Cauchy-Schwarz inequality.

## SI Metric Conversion Factors

| | |
|---|---|
| bbl $\times$ 1.589 873 | E−01 = $m^3$ |
| $ft^3$ $\times$ 2.831 685 | E−01 = $m^3$ |
| psi $\times$ 6.894 757 | E+00 = kPa |

**SPERE**

---

**Robert Eymard** heads the Modeling Dept. at Laboratoire Central des Ponts & Chaussées in Paris and is a professor of mathematics at Paris-Nord U. Before that, he was a reservoir engineer and then worked as an expert in numerical methods at Elf Aquitaine. Eymard holds a PhD in mathematics from the U. of Savoie, France. **Fernand Sonier** is head of Simulation & Modelling Consultancy Ltd. in London. Previously, he worked for Scientific-Software-Intercomp as a development consultant and for Franlab and Inst. Français du Pétrole. He holds an MS degree in applied mathematics from Grenoble U., France.

Eymard Sonier